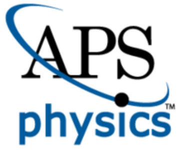

This is the accepted manuscript made available via CHORUS. The article has been published as:

Giant Edelstein effect in topological-insulator–graphene heterostructures

M. Rodriguez-Vega, G. Schwiete, J. Sinova, and E. Rossi

Phys. Rev. B **96**, 235419 — Published 13 December 2017

DOI: 10.1103/PhysRevB.96.235419

Giant Edelstein effect in Topological-Insulator–Graphene heterostructures

M. Rodriguez-Vega
Department of Physics, College of William and Mary, Williamsburg, VA 23187, USA and
Department of Physics, Indiana University, Bloomington, Indiana 47405, USA

G. Schwiete
Department of Physics and Astronomy, Center for Materials for Information Technology (MINT),
The University of Alabama, Alabama 35487, USA

J. Sinova
Institut für Physik, Johannes Gutenberg Universitat Mainz, 55128 Mainz, Germany. and
Institute of Physics, Academy of Sciences of the Czech Republic,
Cukrovarnicka 10, 162 53 Praha 6 Czech Republic

E. Rossi
Department of Physics, College of William and Mary, Williamsburg, VA 23187, USA
(Dated: December 4, 2017)

The control of a ferromagnet's magnetization via only electric currents requires the efficient generation of current-driven spin-torques. In magnetic structures based on topological insulators (TIs) current-induced spin-orbit torques can be generated. Here we show that the addition of graphene, or bilayer graphene, to a TI-based magnetic structure greatly enhances the current-induced spin density accumulation and significantly reduces the amount of power dissipated. We find that this enhancement can be as high as a factor of 100, giving rise to a giant Edelstein effect. Such a large enhancement is due to the high mobility of graphene (bilayer graphene) and to the fact that the graphene (bilayer graphene) sheet very effectively screens charge impurities, the dominant source of disorder in topological insulators. Our results show that the integration of graphene in spintronics devices can greatly enhance their performance and functionalities.

I. INTRODUCTION

The ability to generate and control spin currents in condensed matter systems has led to several discoveries of great fundamental and technological interest [1,2]. In recent years the discovery of whole new classes of materials with strong spin-orbit coupling, such as topological insulators (TIs)[3,4], has allowed the realization of novel basic spin-based phenomena[5–8].

In a system with spin-orbit coupling (SOC), a charge current (I) can induce a spin-Hall effect (SHE)[2] i.e. a pure spin-polarized current. A companion effect to the SHE, also arising from the SOC, is the inverse spin-galvanic effect (ISGE), where a current induces a non-equilibrium uniform spin accumulation[2,9–11]. In a magnetic system this current-driven spin accumulation results in a spin-orbit torque (SOT) acting on the magnetization ($\mathbf{M}$), and therefore can be exploited to realize current-driven magnetization dynamics. The SOT, $\boldsymbol{\tau}_{SO}$, can be either an (anti-)damping torque[2,12], i.e. have the same functional form as the Gilbert damping term, or *field-like*[2], i.e. have the form $\boldsymbol{\tau}_{SO} = \gamma \mathbf{B}_{SO} \times \mathbf{M}$, where $\mathbf{B}_{SO}$ is an effective spin-orbit field, and γ is the gyromagnetic ratio. The presence of a current-driven SOT on the surface of TIs has been predicted[13–17] and it has been recently measured in TI-ferromagnet bilayers[18] and magnetically doped TIs[19].

The two-dimensional nature of graphene (SLG) and bilayer graphene (BLG)[20–22] and the fact that their

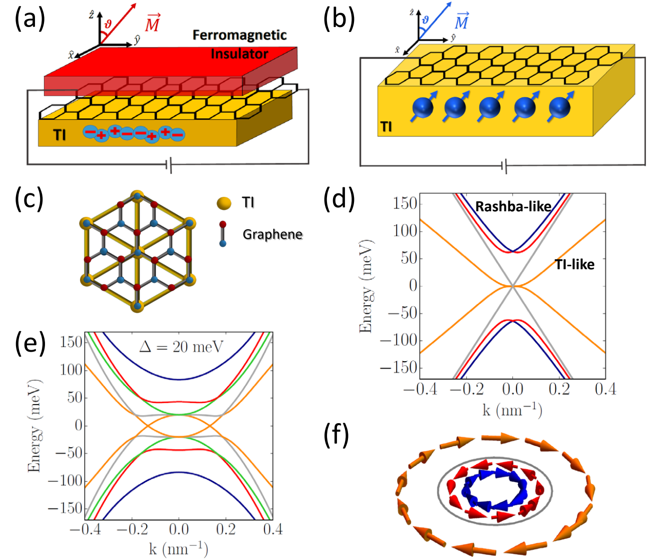

FIG. 1. Sketch of a TI-graphene-FM, (a), and of a magnetically doped TI-graphene, (b), heterostructure. In (a) the random charges are shown. In (b) the spheres represent magnetic dopant, the random charges are not shown explicitly. (c) Atoms' arrangement for the commensurate stacking considered. (d) Bands for TI-SLG for $\Delta = 0$, $\delta\mu = 0$. (e) Bands for TI-BLG for $\Delta = 20$ meV and $\delta\mu = 0$. (f) Spin texture on the Fermi surface formed by the bands shown in (d) for $\epsilon_F = 100$ meV.

room-temperature mobilities are higher than in any other known material[23] make them extremely interesting for transport phenomena. However, the SOC in graphene is extremely small and as a consequence graphene alone is not very interesting for spintronics applications, except as a spin-conductor. Several methods have been proposed to induce larger SOC in graphene[24]. Recent experiments on TI-graphene heterostructures seem to demonstrate the injection of spin-polarized current from a TI into graphene[25,26].

In this work we show that the combination of a particular class of three-dimensional (3D) TIs and graphene allows the realization of devices in which a charge current induces a spin density accumulation that can be up to a factor 100 larger than in any previous system, i.e. a *giant Edelstein effect*. We find that for most of the experimentally relevant conditions considered the SOT in TI-graphene vdW heterostructures should be higher than the already very large values observed in TI-Ferromagnet bilayers[18] and magnetically doped TIs[19]. In Ref. 18, for $I = 7.7$ mA, a $B_{SO} = 3 \times 10^{-2}$ mT was measured, in Ref. 19, for $I = 4\mu$A, a $B_{SO} = 80$ mT was measured[27]. Assuming that our work is able to capture the key elements affecting the SOT in TI-graphene systems we find that in these systems the SOT could be ten times larger than the values found in Ref. 18 and 19. We also find that TI-SLG and TI-BLG systems have conductivities much higher than TI surfaces and would therefore allow the realization of spintronics effects with dramatically lower dissipation than in TIs alone.

The rest of the paper is organized as follows: in Sec. II we introduce the effective model for the TI-graphene heterostructure, describe the treatment of disorder, and outline the calculation of the current-induced spin density response function; in Sec. III we present our results; finally, in Sec. IV we present our conclusions.

II. THEORETICAL FRAMEWORK

In vdW heterostructures[28], the different layers are held together by vdW forces. This fact greatly enhances the type of heterostructures that can be created given that the stacking is not fixed by the chemistry of the elements forming the heterostructure. With $a = 2.46\AA$ being the lattice constant of graphene, and a_{TI} the lattice constant of the 111 surface of a TI in the tetradymite family, we have $a_{TI}/a = \sqrt{3}(1+\delta)$, where $\delta < 1\%$ for Sb_2Te_3, $\delta = -3\%$ for Bi_2Se_3, and $\delta = 3\%$ for Bi_2Te_3. As a consequence, graphene and the 111 surface of Sb_2Te_3, Bi_2Se_3, Bi_2Te_3, to very good approximation, can be arranged in a $\sqrt{3}\times\sqrt{3}$ commensurate pattern [29–31]. When the stacking is commensurate the hybridization between the graphene's and the TI's surface states is maximized. This property of graphene, combined with its high mobility, its intrinsic two-dimensional nature, and its ability at finite dopings to effectively screen the dominant source of disorder in TIs, make graphene the ideal material to consider for creating a TI heterostructure with a very large Edelstein effect.

TI-graphene heterostructures can be formed via mechanical transfer[26,32,33]. As a consequence, the stacking pattern and the shift are fixed by the exfoliation-deposition process and can be controlled[34]. Density functional theory (DFT) results show that the binding energy between graphene and the TIs surface depends only very weakly on the rigid shift[29,35–37]. Among the commensurate configurations with free energy close to the minimum, as obtained from DFT calculations[29], we consider the stacking configuration shown in Fig. 1 (c). For this configuration, we expect the Edelstein effect to be the smallest because the graphene bands split into Rashba-like bands (see Figs. 1 (d), (e)), that give an Edelstein effect with opposite sign to the one given by TI-like bands[18]. Therefore, to be conservative, in the remainder we consider both the commensurate case for which the Edelstein effect is expected to be the weakest (i.e., the case in the graphene sublattice symmetry is broken) and the extreme case in which the tunneling strength between the TI and graphene is set to zero.

At low energies, the Hamiltonian for the system can be written as $H = \sum_{\mathbf{k}} \psi^\dagger_{\mathbf{k}} H_{\mathbf{k}} \psi_{\mathbf{k}}$ where $\psi^\dagger_{\mathbf{k}}$ ($\psi_{\mathbf{k}}$) is the creation (annihilation) spinor for a fermionic excitation with momentum $\mathbf{k}$, and

$$\mathrm{H}_{\mathbf{k}} = \begin{pmatrix} \hat{H}^{G,K}_{\mathbf{k}} & 0 & \hat{T}^\dagger \\ 0 & \hat{H}^{G,K'}_{\mathbf{k}} & \hat{T}^\dagger \\ \hat{T} & \hat{T} & \hat{H}^{TI}_{\mathbf{k}} \end{pmatrix}, \quad \hat{\mathrm{T}} = \begin{pmatrix} t & 0 & 0 & 0 \\ 0 & 0 & t & 0 \end{pmatrix}, \tag{1}$$

where $\hat{H}^{G,K}_{\mathbf{k}}$ ($\hat{H}^{G,K'}_{\mathbf{k}} = [\hat{H}^{G,K}_{\mathbf{k}}]^*$) is the Hamiltonian describing graphene's low energy states around the K (K') of the Brillouin zone. For SLG $\hat{H}^{G,K}_{\mathbf{k}} = \hat{H}^{SLG,K}$ and for BLG $\hat{H}^{G,K}_{\mathbf{k}} = \hat{H}^{BLG,K}$. $\hat{H}^{TI}_{\mathbf{k}}$ is the Hamiltonian describing the TI's surface states, and $\hat{T}$ is the matrix describing spin- and momentum- conserving tunneling processes between the graphene layer and the TI's surface[31], t being the tunneling strength. The TI's bulk states are assumed to be gapped. This condition is realized, for example, in novel ternary or quaternary tetradymites, such as Bi_2Te_2Se and $Bi_{2-x}Sb_xTe_{3-y}Se_y$, for which it has been shown experimentally that the bulk currents have been completely eliminated[38–45]. For SLG we have $\hat{H}^{SLG,K}_{\mathbf{k}} = \hbar v_g k \sigma_0 [\cos(\phi_{\mathbf{k}})\tau_x + \sin(\phi_{\mathbf{k}})\tau_y] - \mu_g$, where $v_g \approx 10^6$ m/s is the graphene's Fermi velocity, $k = |\mathbf{k}|$, $\phi_{\mathbf{k}} = \arctan(k_y/k_x)$, σ_i, τ_i are the Pauli matrices in spin and sublattice space respectively, and μ_g is the chemical potential. For BLG we have $\hat{H}^{BLG,K}_{\mathbf{k}} = \hbar^2 k^2/(2m^*)\sigma_0 [\cos(2\phi_{\mathbf{k}})\tau_x + \sin(2\phi_{\mathbf{k}})\tau_y] - \mu_g$, where $m^* \approx 0.035 m_e$ is the effective mass. For the TI's surface states, we have $\hat{H}^{TI}_{\mathbf{k}} = \hbar v_{TI}(k_y\sigma_x - k_x\sigma_y) - \mu_{\rm TI}\sigma_0$, where $v_{TI} \approx v_g/2$ and $\mu_{\rm TI}$ is the chemical potential on the TI's surface . In the remainder the Fermi energy ϵ_F is measured from the neutrality point of the SLG (or the BLG) and $\delta\mu \equiv \mu_{TI} - \mu_g$.

In a magnetically doped TI, below the Curie temper-

ature, the low energy Hamiltonian for the TI-graphene's quasiparticles, Eq. (1), has an additional term, H_{ex}, describing the exchange interaction between the quasiparticles and the magnetization $\mathbf{M}$. $H_{ex} = \Delta \int_\Omega \hat{\mathbf{m}} \cdot \hat{\mathbf{s}}\, d\mathbf{r}/\Omega$, where Δ is the strength of the exchange interaction, $\hat{\mathbf{m}} \equiv \mathbf{M}/|\mathbf{M}|$, $\hat{\mathbf{s}} \equiv \mathbf{s}/|\mathbf{s}|$ with $\mathbf{s}$ the TI-graphene's spin density operator, and Ω is the 2D area of the sample. For a TI-graphene-ferromagnet heterostructure the ferromagnet (FM) will also cause simply the addition of the term H_{ex} to the Hamiltonian for the quasiparticles, Eq. (1), as long as the FM is an insulator, and is placed on graphene, or bilayer graphene, via mechanical exfoliation, likely with a large twist angle to minimize hybiridization. Recent experiments have studied $\mathrm{Bi_2Se_3} - \mathrm{EuS}$ systems[46,47]. In the remainder, for TI-graphene-FM heterostructures we assume the FM to be an insulator.

To maximize the effect of the current-induced spin accumulation on the dynamics of the magnetization, it is ideal to have $\mathbf{M}$ perpendicular to the TI's surface. This is the case for magnetically doped TIs such as $\mathrm{Cr_{2x}(Bi_{0.5}Sb_{0.5-x})_2Te_3}$[19]. For TI-graphene-FM trilayers this can be achieved, for example, by using a thin film of $\mathrm{BaFe_{12}O_{19}}$, a magnetic insulator with high T_c and large perpendicular anisotropy[48].

By comparing the bands for TI-SLG, at low-energies, obtained from Eq. (1), Fig. 1 (d), with the ones obtained using DFT[29,36,37] we obtain that the effective value of t is $\sim$ 45 meV. For this reason, most of the results that we show in the remainder were obtained assuming $t =$ 45 meV. Fig. 1 (d) clearly shows that, in general, the hybridization of the graphene's and TI's states preserves a TI-like band and induces the formation of spin-splitted Rashba bands. The TI and Rashba nature of the bands can clearly be evinced from the winding of the spins, as shown in Fig. 1 (f). The same qualitative features can be observed in Fig. 1 (e) that shows the low energy bands of a TI-BLG system with $\Delta = 20$ meV, and $\delta\mu = 0$.

In the remainder, we restrict our analysis to the case in which ϵ_F is such that the system is metallic. In this case contributions to the Edelstein effect from interband-transitions[49] can be neglected and the SOT is primarily field-like. For most of the conditions of interest, quantum interference effects can be assumed to be negligible due to dephasing effects at finite temperatures and the large dimensionless conductance of the system. The SOT can be obtained by calculating the current-induced spin density accumulation $\delta s^i = \chi^{s_i J_j}(\mathbf{q},\omega) E^j$, where E^j is the electic field applied in the j-direction and the spin density response function $\chi^{s_i J_j}(\mathbf{q},\omega)$, within the linear response regime, is equal to the spin-current correlation function. Considering that the SOT is given by $\mathbf{B_{so}} \times \mathbf{M}$, where $\mathbf{B_{so}} = \delta\mathbf{s}$ is the effective spin-orbit field due to the Edelstein effect, and that the response function depends weakly on the gap Δ induced by $\mathbf{M}$ (see Fig. (5)), the angular dependence of the torque is mainly geometrical. Without loss of generality, we can assume the external current to be in the y direction so that $\delta\mathbf{s} \parallel \hat{x}$ and therefore $\boldsymbol{\tau}_{SO} \approx |\mathbf{M}| \delta s^x \cos\vartheta\, [-\hat{y} + \hat{z} \tan\vartheta \sin\phi]$, where ϑ is the angle formed by the magnetization and the TI's surface (see Fig. (1a)) and ϕ is the angle with respect to $\hat{x}$ in the TI surface plane.

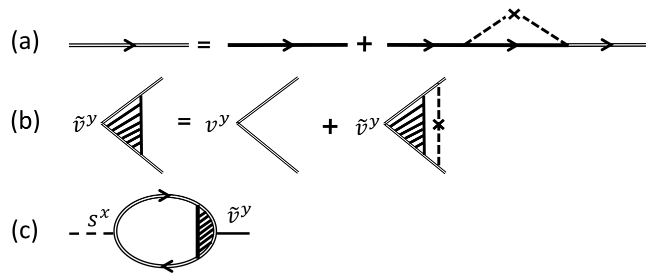

FIG. 2. Diagrams used to calculate the charge conductivity and the spin-current response.

The unavoidable presence of disorder induces a broadening of the quasiparticle states, and vertex corrections that are captured by the diagrams shown in Fig. 2. In TIs charge impurities appear to be the dominant source of disorder[50] and so it is expected that they will also be in TI-graphene heterostructures. We therefore model the disorder as a random potential created by an effective 2D distribution of uncorrelated charge impurities with zero net charge placed at an effective distance d below the TI's surface. Direct imaging experiments[51] suggest $d \approx 1$ nm, consistent with transport results[50,52].

In momentum space, the bare potential $v(q)$ created on the TI's surface by a single charge impurity is $v(q) = 2\pi e^2 e^{-qd}/(\kappa q)$ where $\kappa = (\kappa_{TI} + \kappa_0)/2$ is the average dielectric constant with $\kappa_{TI} \approx 100$ [50–54] the dielectric constant for the TIS and $\kappa_0 = 1$ the dielectric constant of vacuum[55]. The screened disorder potential is $v(q)/\epsilon(q)$ where $\epsilon(q)$ is the dielectric function[23,56,57]. To obtain the current-driven SOT in the dc limit, and for temperatures T much lower than the Fermi temperature T_F, to very good approximation we can assume $\epsilon(q) \approx 1 + v_c(q)\nu(\epsilon_F)$, where $v_c(q) = 2\pi e^2/(\kappa q)$ and $\nu(\epsilon_F)$ is the density of states at the Fermi energy.

The lifetime $\tau_{0a}(\mathbf{k})$ of a quasiparticle in band a with momentum $\mathbf{k}$ is given by

$$\frac{\hbar}{\tau_{0a}(\mathbf{k})} = 2\pi \sum_{a'\mathbf{q}} n_{\rm imp} \left|\frac{v(q)}{\epsilon(q)}\right|^2 |\langle a'\mathbf{k}+\mathbf{q}|a\mathbf{k}\rangle|^2 \delta(\epsilon_{a,\mathbf{k}} - \epsilon_{a',\mathbf{k}+\mathbf{q}}), \tag{2}$$

where $n_{\rm imp}$ is the impurity density and $|a\mathbf{k}\rangle$ is the Bloch state with momentum $\mathbf{k}$ and band index a. In the remainder, we set $n_{\rm imp} = 10^{12}\mathrm{cm}^{-2}$.[50] The transport time $\tau_{ta}(\mathbf{k})$, that renormalizes the expectation value of the velocity operator, is obtained by introducing the factor $[1 - \mathbf{k}\cdot(\mathbf{k}+\mathbf{q})]$ under the sum on the right hand side of Eq. (2), and in general differs from the lifetime $\tau_{0a}(\mathbf{k})$[58–62].

For a charge current in the y direction the non equilibrium spin density is polarized in the x direction, as shown schematically in Fig. 4 (a). Due to the rotational symmetry of the system we have $\chi^{s_x J_y} = -\chi^{s_y J_x}$ and

$\chi^{s_x J_x} = \chi^{s_y J_y}$. Without loss of generality we can assume the current to be in the y direction. Within the linear response regime, taking into account the presence of disorder, the response function $\chi^{s_x J_y}$ of the system can be obtained by calculating the diagrams shown in Fig. (2). The diagram in Fig. (2a) represents the equation for the self-energy in the first Born approximation, where the double line represents the disorder-dressed electrons' Green's function, the single line the electron's Green's function for the clean system, and the dashed lines scattering events off the impurities. The diagram in Fig. (2b) corresponds to the equation for the renormalized velocity vertex, $\tilde{v}_y$, at the ladder level approximation. In the long wavelength, dc, limit we have

$$\chi^{s_x J_y} \approx \frac{e}{2\pi\Omega} \mathrm{Re} \sum_{\mathbf{k},a} s^x_{aa}(\mathbf{k}) \tilde{v}^y_{aa}(\mathbf{k}) G^A_{\mathbf{k}a} G^R_{\mathbf{k}a} \,, \qquad (3)$$

where $s^i_{aa}(\mathbf{k}) \equiv \langle a\mathbf{k}|s_i|a\mathbf{k}\rangle$ is the expectation value of the i-th component of the spin density operator, $\tilde{v}^i_{aa}(\mathbf{k}) = (\tau_a/\tau_{0a})_{\mathbf{k}} v^i_{aa}(\mathbf{k})$ with $v^i_{aa}(\mathbf{k}) \equiv \langle a\mathbf{k}|v_i|a\mathbf{k}\rangle$ the expectation value of the i-th component of the velocity operator $\mathbf{v} = \hbar^{-1}\partial H_{\mathbf{k}}/\partial\mathbf{k}$, and $G^{R/A}_{\mathbf{k}a} = (\epsilon_F - \epsilon_{\mathbf{k}a} \pm i\hbar/2\tau_{0a}(\mathbf{k}))^{-1}$ are the retarded and advanced Green's functions, respectively, for electrons with momentum $\mathbf{k}$ and band index a.

III. RESULTS

In this section, we present our results for the transport properties and current-induced spin density accumulation of TI-graphene heterostructures.

We define the average τ_0, τ_t as $\langle\tau_{0(t)}(\epsilon_F)\rangle \equiv \sum_{\mathbf{k}a} \tau_{0a(ta)}(\mathbf{k})\delta(\epsilon_F - \epsilon_{\mathbf{k}a}) / \sum_{\mathbf{k}a} \delta(\epsilon_F - \epsilon_{\mathbf{k}a})$. Figs. 3 (a), (b) show $\langle\tau_0(\epsilon_F)\rangle$, and $\langle\tau_t(\epsilon_F)\rangle$, respectively, for a TI's surface, a TI-SLG heterostructure, and a TI-BLG heterostructure, with $\Delta = 0$ meV. We see that the presence of a graphene layer strongly increases both $\langle\tau_0(\epsilon_F)\rangle$, and $\langle\tau_t(\epsilon_F)\rangle$, and that such increase is dramatic for the case when the layer is BLG. $\langle\tau_0(\epsilon_F)\rangle$, and $\langle\tau_t(\epsilon_F)\rangle$ are larger in BLG-TI than TI-SLG because, especially at low energies, BLG has a larger density of states than SLG causing $\varepsilon(q)$, that enters in the denominator in Eq. (2), and therefore $\langle\tau_0(\epsilon_F)\rangle$, and $\langle\tau_t(\epsilon_F)\rangle$ to be larger in BLG than in SLG. Notice that τ_0, τ_t increase after adding a graphene layer even in the limit when $t = 0$ as shown by the dashed lines in Fig. 3. This is due to the fact that the graphene layer screens the dominant source of disorder in the TI even when $t = 0$. Changes in Δ have only minor quantitative effects as long as $\Delta < (t, \epsilon_F)$.

Figure 4 (a) shows the dependence of $\chi^{s_x J_y}$ on ϵ_F for TI, TI-SLG, and TI-BLG for $t = 45$ meV, $\delta\mu = 0$ and $\Delta = 20$ meV with out-of-plane magnetization $\hat{m} = \hat{z}$ (solid lines). The dashed lines corresponds to the case $\Delta = 0$. The inset shows a sketch of the system, with charge flowing in the y-direction. The direction of the spin accumultion on the top and bottom layer is indicated by the arrows on the electrons. The insertion of a graphene layer strongly enhances the current-induced spin density response and therefore the SOT. Now, we consider in-plane magnetization. In this case, the Fermi surface is not isotropic as for out-of-plane magnetization, which makes the computation of scattering time, transport times, and the Edelstein effect more challenging. For concreteness, we assume the magnetization direction to be $\hat{m} = \hat{x}$ ($\|$). Fig. 4 (b) shows $\chi^{s_x J_y}$ as a function of ϵ_F for in-plane $\hat{m} = \hat{x}$ ($\|$) magnetization and $\Delta = 20$ meV, dashed lines. The red lines correspond to a TI-BLG-FM and the black lines to a TI-FM heterostructure. We obtained an enhancement as large as the one obtained for out-of-plane magnetization $\hat{m} = \hat{z}$ ($\perp$), solid lines.

We find that changes in $\delta\mu$ have a strong impact on $\chi^{s_x J_y}$. Figure 4 (c) shows that by increasing $\delta\mu$ the enhancement of the SOT can be raised to values as high as 100 in TI-BLG heterostructures due to the flattening and consequent increase of the DOS of the TI-like bands (see Appendix A). The results of Fig. 4 show that in TI-SLG and TI-BLG heterostructures the current-induced SOT can be expected to be much higher than in TI surfaces alone. They show that for TI-BLG systems there is a large range of values of $\delta\mu$, ϵ_F for which the enhancement of $\chi^{s_x J_y}$ due to the presence of the BLG is consistently close to 10 or larger, Fig. 4 (c).

We also find that the strong enhancement of $\chi^{s_x J_y}$ is not affected significantly by the value of Δ, as shown in Fig. (5), where we plot $\chi^{s_x J_y}$ as a function of Δ at $\epsilon_F = 60$ meV. In Fig. (5) (a) we plot $\chi^{s_x J_y}$ for TI-FM, while (5) (b) shows the response function $\chi^{s_x J_y}$ for TI-SLG(BLG)-FM normalized to the response in a TI-FM system.

In addition, in a TI-graphene heterostructure, by placing the source and drain on the graphene (BLG) and taking into account the high mobility of graphene (BLG), it is possible to force most of the current to flow within graphene (BLG) and the TI's surface adjacent to it. Therefore, we can minimize the amount of spin density accumulation with opposite polarization that a current flowing in the TI's bottom surface generates. This fact should further increase the net SOT.

The large enhancement of the spin density accumulation in TI-graphene systems is due to two main reasons:

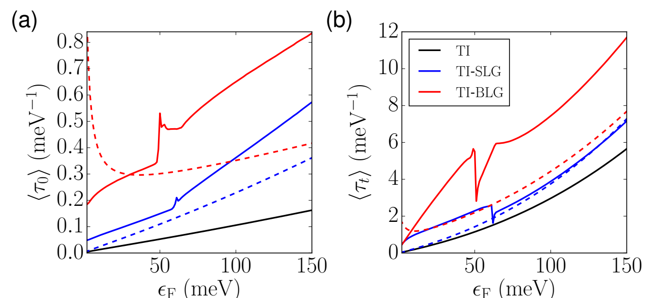

FIG. 3. (a) $\langle\tau_0(\epsilon_F)\rangle$, and (b) $\langle\tau_t(\epsilon_F)\rangle$ for $\Delta = 0$ meV, $\delta\mu = 0$ meV, and $n_{\rm imp} = 10^{12}$ cm^{-2}. The solid lines correspond to $t = 45$ meV while dashed lines to the limit $t = 0$ meV.

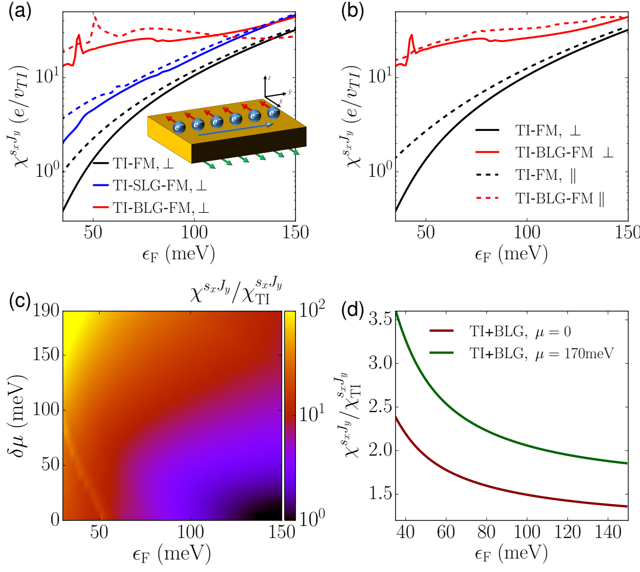

FIG. 4. (a) $\chi^{s_x J_y}$ as a function of ϵ_F for $\delta\mu = 0$, $t = 45$ meV, and $\Delta = 20$ meV ($\Delta = 0$) with out-of-plane magnetization $\hat{m} = \hat{z}$ ($\perp$), solid (dashed) lines. Inset: sketch showing the spin density accumulation on the top and bottom surface of a TI induced by a current in the y direction. (b) $\chi^{s_x J_y}$ as a function of ϵ_F for in-plane $\hat{m} = \hat{x}$ ($\|$) (out-of-plane $\hat{m} = \hat{z}$ ($\perp$)) magnetization and $\Delta = 20$ meV, dashed (solid) lines. The other parameters are the same as in (a). (c) Enhancement of $\chi^{s_x J_y}$ in a TI-BLG system compared to TI alone as a function of ϵ_F and $\delta\mu$ for $\Delta = 0$. (d) $\chi^{s_x J_y}$ for TI-BLG when $t = 0$. In all the panels, the disorder parameters are $n_{\rm imp} = 10^{12}$ cm^{-2}, and $d = 1$ nm.

(i) the survival, after hybridization, of TI-like bands well separated from Rashba bands; (ii) the strong enhancement of the relaxation time τ_0 and transport time τ_t due to the additional screening by the graphene layer of the dominant source of disorder. It is important to notice that the presence of the Rashba bands, see Fig. 1, not only is not essential for the enhancement of the spin density accumulation but it can be detrimental given that the Rashba bands give a $\chi^{s_x J_y}$ with opposite sign of the TI-like bands. This fact can be seen at large Fermi energies for BLG-TI in Fig. 4 (b): for $\epsilon_F \gtrsim 140$ meV the Fermi surface intersect the Rashba bands that by giving a contribution to $\chi^{s_x J_y}$ opposite to the TI-like bands brings the net SOT of TI-BLG to be slightly lower than the SOT of TI-alone. Point (ii) explains the fact the $\chi^{s_x J_y}$, at low energies, is always larger in TI-BLG rather than TI-SLG given that τ_0 and τ_t are larger in TI-BLG than in TI-SLG. In addition, it explains the fact that even in the limit when there is no hybridization between the TI and the graphene bands, i.e. t=0 due for example to a large twist angle (see Appendix B), the spin-current correlation function in TI-graphene systems is still larger than in TIs alone for the experimentally relevant case where charge impurities are the dominant source of disorder, as shown in Fig. 4 (d).

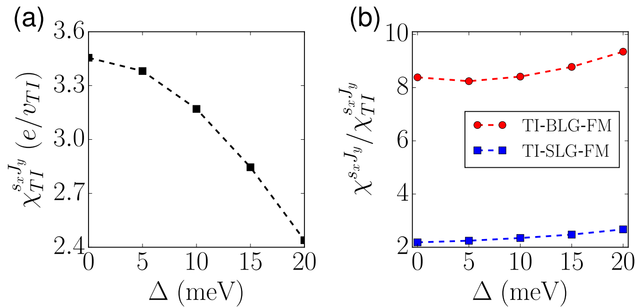

FIG. 5. (a) $\chi^{s_x J_y}$ as a function of the exchange interaction Δ for a TI-FM heterostructure at $\epsilon_F = 60$ meV. (b) Ratio $\chi^{s_x J_y}/\chi^{s_x J_y}_{TI}$ of the TI-BLG-FM (red circles) and TI-SLG-FM (blue squares) response to the TI-FM response. The magnetization direction is out-of-plane, $\hat{m} = \hat{z}$ ($\perp$).

In Fig. 6 (a), we show the current-induced spin density accumulation response function dependence on the tunneling amplitude t, normalized to the TI response. As t is increased, TI and graphene hybridize more strongly, leading to a larger SOT. However, even at vanishing tunneling, an enhancement is still present.

In Fig. 6 (b), we plot $\chi^{s_x J_y}$ as a function of the effective distance from the TI surface to the effective layer of impurities d. The further away the impurities are located, the weaker the disorder, and therefore the larger the expected SOT.

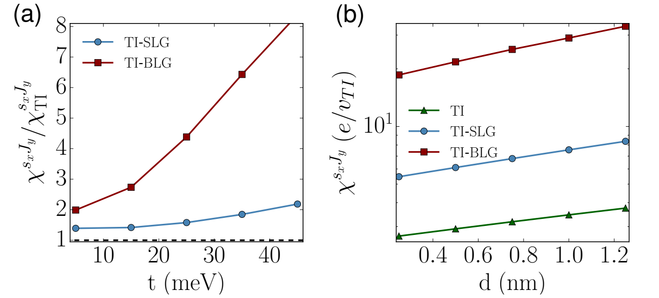

FIG. 6. (a) $\chi^{s_x J_y}/\chi^{s_x J_y}_{TI}$ as a function of the tunneling amplitude t for TI-SLG and TI-BLG heterostructures at $\epsilon_F = 60$ meV and $\delta\mu = 0$. (b) $\chi^{s_x J_y}$ as a function of the effective distance to the impurities d for TI-SLG and TI-BLG heterostructures at $\epsilon_F = 60$ meV and $\delta\mu = 0$.

To estimate the efficiency of the current-induced SOT in TI-graphene heterostructures, we calculate the associated dc longitudinal conductivity σ^{ii} for the same parameters. In the linear-response, long-wavelength, regime we have

$$\sigma^{ii} \approx \frac{e^2}{2\pi\Omega} \,\mathrm{Re} \sum_{\mathbf{k},a} v^i_{aa}(\mathbf{k}) \tilde{v}^i_{aa}(\mathbf{k}) G^A_{\mathbf{k}a} G^R_{\mathbf{k}a} \,. \tag{4}$$

Fig. 7 (a) shows σ^{yy} for TI, TI-SLG, and TI-BLG as a function of ϵ_F in the limit $\Delta = 0$. We see that the presence of a graphene layer enhances the conductivity of

the system by an order of magnitude or more. Fig. 7 (b) shows that the exchange term H_{ex} does not affect σ^{yy} significantly. The results shown in Fig. 7 (b) imply that in TI-graphene heterostructures not only the current-induced SOT can be much larger than in TIs alone, but also that the generation of the SOT is much less dissipative. For example, for an applied electric fields of the order of 0.1 V/μm, we can reach a conservative spin density accumulation $\delta s^x \approx 5\times 10^7\hbar$ cm^{-2}. For typical carrier density in graphene ($n\approx 10^{11}$cm^{-2}), we have $\delta s^x/n = 5\times 10^{-4}\hbar$.

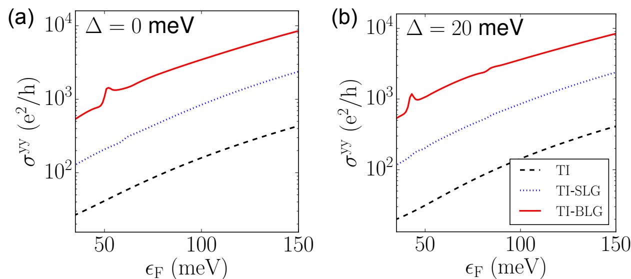

FIG. 7. $\sigma^{yy}(\epsilon_F)$, for TI (dashed line), TI-SLG (dotted line), and TI-BLG (solid line) for $\Delta = 0$, (a), and $\Delta = 20$ meV (b) with out-of-plane magnetization, $\hat{m} = \hat{z}$ ($\perp$). $t = 45$ meV, $\delta\mu = 0$, and $n_{\rm imp} = 10^{12}$ cm^{-2}.

IV. CONCLUSIONS

In conclusion, we have shown that in magnetic TI-graphene heterostructures the non-equilibrium uniform spin density accumulation induced by a charge current can be 10-100 times higher than in TIs alone giving rise to a giant Edelstein effect. The reasons for these enhancements are (i) the additional screening by the graphene layer of the dominant source of disorder; (ii) the fact that graphene and the TI's surface are almost commensurate making possible a strong hybridization of the TI's and graphene's states; (iii) the fact that the spin structure of the hybridized bands has a spin structure very similar to the one of the original TI's band for a large range of dopings; (iv) the fact that graphene is the ultimate 2D system, only one-atom thick. These facts and our results suggest the TI-graphene systems are very good candidates to realize all-electric efficient magnetization switching.

ACKNOWLEDGEMENTS

We acknowledge helpful discussions with Yong Chen and Saroj Dash. MRV and ER acknowledge support from NSF Grant No. DMR-1455233 and ONR Grant No. N00014-16-1-3158. ER also acknowledges support from ARO Grant No W911NF-16-1-0387, and the United States-Israel Binational Science Foundation, Jerusalem, Israel. In addition, MRV and ER thank the hospitality of the Spin Phenomena Interdisciplinary Center (SPICE), where this project was initiated. JS and GS acknowledge the support by Alexander von Humboldt Foundation, the ERC Synergy Grant SC2 (No. 610115), and the Transregional Collaborative Research Center (SFB/TRR) 173 SPIN+X.

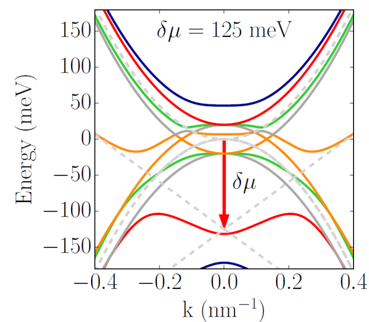

FIG. 8. TI-BLG band structure for $\delta\mu = 125$ meV, and tunneling amplitude $t = 45$ meV.

Appendix A: TI-BLG BAND STRUCTURE

As long as the interlayer tunneling t_{BLG} between the carbon atoms in bilayer graphene is much larger than the expected tunneling t between the TI's surface and the graphenic layer any difference between the tunneling strength between the carbon layers forming BLG and the TI will give very negligible effects. Considering that in bilayer graphene the interlayer tunneling is 350 meV, and the fact that for the TI-graphene tunneling t we only consider values smaller than 45 meV for all our results is $t \ll t_{BLG}$. In this limit, at low energies ($\lesssim 350$ meV), BLG can be treated as 2D system with the effective Hamiltonian H^{BLG} presented in the main text.

Fig. 1 (e) in the main text shows the bands of a TI-BLG systems for which the exchange field $\Delta = 20$ meV and $\delta\mu = 0$. Fig 3 shows that the strongest enhancement of the SOT happens for TI-BLG systems when $\delta\mu \neq 0$. It is therefore interesting to see how the low-energy bands of TI-BLG are affected by a nonzero value of $\delta\mu$. Fig. 8 shows the band structure of TI-BLG for the case when $\delta\mu = 125$ meV in the absence of any exchange field. We see that one of TI-like bands (shown in orange) becomes much flatter: the high density of states of this band explains the high values of SOT for TI-graphene systems when $\delta\mu \neq 0$.

Appendix B: INVERSE SPIN GALVANIC EFFECT IN TWISTED TI-GRAPHENE HETEROSTRUCTURES

It can expected that even when the stacking of the graphenic layer and the TI's surface is incommensurate, the screening of the charge impurities by the graphenic layer will lead to a strong enhancement of τ_0 and τ_t and therefore of the SOT. The accurate treatment of the realistic case in which the main source of disorder are charge impurities for incommensurate stackings requires the calculation of the dielectric constant for incommensurate structures, a task that is beyond the scope of the present work. For this reason, to exemplify how the presence of a small twist angle θ between the graphenic layer and the TI surface, giving rise to an incommensurate stacking, affects the calculation of the SOT, we consider a very simple model for the effect of the disorder: we simply assume that the disorder gives rise to a constant quasiparticle broadening.

Let $|\mathbf{q}| \equiv q = 2K_D \sin(\theta/2)$, where K_D is the magnitude of the graphene K point. The dimensionless parameter $\gamma \equiv \frac{t'}{\hbar v_{TI} q}$, where $t' = t/3$, measures the strength of the coupling between the graphenic layer and the TIS. For $\gamma < 1$ we can obtain the electronic structure using the weak coupling theory for twisted systems[63–65] that for the case of a TI-graphene heterostructures we presented in Ref.[31]. After obtaining the electronic structure in the regime $\gamma < 1$, we can obtain $\chi^{s_x J_y}$. To understand how the response between the commensurate and the incommensurate regimes differ, we have calculated $\chi^{s_x J_y}$ assuming a constant quasiparticle broadening $1/(2\tau_0) = 2$ meV, with $t' = 15$ meV, $\delta\mu = 0$, and $\epsilon_F = 10$ meV for a range of values of θ for which the weak coupling theory is valid. The dependence of $\chi^{s_x J_y}$, per valley, as a function of θ for TI-SLG and TI-BLG is shown in Fig. 9. As to be expected, the results show that in the incommensurate case the response is smaller than in the commensurate case. However, they also show, in particular for the case in which the graphenic layer is BLG, that a TI-graphene heterostructure is expected to have stronger $\chi^{s_x J_y}$, and therefore a stronger inverse spin-galvanic effect, even in the incommensurate regime and for the case in which the disorder is modeled very simply.

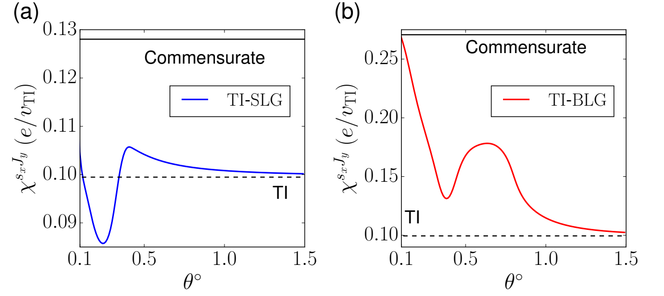

FIG. 9. (a) $\chi^{s_x J_y}$ as a function of twist angle θ for TI-SLG. (b) Same as (a) for TI-BLG.

[1] I. Žutić, J. Fabian, and S. Das Sarma, Rev. Mod. Phys. **76**, 323 (2004).
[2] J. Sinova, S. O. Valenzuela, J. Wunderlich, C. H. Back, and T. Jungwirth, Rev. Mod. Phys. **87**, 1213 (2015).
[3] M. Z. Hasan and C. L. Kane, Rev. Mod. Phys. **82**, 3045 (2010).
[4] X.-L. Qi and S.-C. Zhang, Rev. Mod. Phys. **83**, 1057 (2011).
[5] J. Sinova and I. Žutić, Nature Materials **11**, 368 (2012).
[6] A. Brataas, A. D. Kent, and H. Ohno, Nature Materials **11**, 372 (2012).
[7] T. Jungwirth, J. Wunderlich, and K. Olejník, Nature Materials **11**, 382 (2012).
[8] G. E. W. Bauer, E. Saitoh, and B. J. van Wees, Nature Materials **11**, 391 (2012).
[9] M. Dyakonov and V. Perel, Physics Letters A **35**, 459 (1971).
[10] V. Edelstein, Solid State Communications **73**, 233 (1990).
[11] M. I. Dyakonov (Ed.), *Spin physics in semiconductors*, Springer Series in Solid-State Sciences, Vol. 157 (Springer, New York, 2008).
[12] H. Kurebayashi, J. Sinova, D. Fang, A. C. Irvine, T. D. Skinner, J. Wunderlich, V. Novák, R. P. Campion, B. L. Gallagher, E. K. Vehstedt, L. P. Zârbo, K. Výborný, A. J. Ferguson, and T. Jungwirth, Nature Nanotechnology **9**, 211 (2014).
[13] I. Garate and M. Franz, Phys. Rev. Lett. **104**, 146802 (2010).
[14] T. Yokoyama, J. Zang, and N. Nagaosa, Phys. Rev. B **81**, 241410 (2010).
[15] A. Sakai and H. Kohno, Phys. Rev. B **89**, 165307 (2014).
[16] M. H. Fischer, A. Vaezi, A. Manchon, and E.-A. Kim, Phys. Rev. B **93**, 125303 (2016).
[17] P. B. Ndiaye, C. A. Akosa, M. H. Fischer, A. Vaezi, E.-A. Kim, and A. Manchon, Phys. Rev. B **96**, 014408 (2017).
[18] A. R. Mellnik, J. S. Lee, A. Richardella, J. L. Grab, P. J. Mintun, M. H. Fischer, A. Vaezi, A. Manchon, E.-A. Kim, N. Samarth, and D. C. Ralph, Nature **511**, 449 (2014).
[19] Y. Fan, X. Kou, P. Upadhyaya, Q. Shao, L. Pan, M. Lang, X. Che, J. Tang, M. Montazeri, K. Murata, L.-T. Chang, M. Akyol, G. Yu, T. Nie, K. L. Wong, J. Liu, Y. Wang, Y. Tserkovnyak, and K. L. Wang, Nature Nanotechnology **11**, 352 (2016).
[20] K. S. Novoselov, A. K. Geim, S. V. Morozov, D. Jiang, M. I. Katsnelson, I. V. Grigorieva, S. V. Dubonos, and A. A. Firsov, Nature **438**, 197 (2005).
[21] Y. Zhang, Y.-W. Tan, H. L. Stormer, and P. Kim, Nature **438**, 201 (2005).
[22] A. H. Castro Neto, F. Guinea, N. M. R. Peres, K. S. Novoselov, and A. K. Geim, Rev. Mod. Phys. **81**, 109 (2009).
[23] S. Das Sarma, S. Adam, E. H. Hwang, and E. Rossi, Rev. Mod. Phys. **83**, 407 (2011).
[24] J. Lee and J. Fabian, Phys. Rev. B **94**, 195401 (2016).
[25] K. Vaklinova, A. Hoyer, M. Burghard, and K. Kern, Nano Letters **16**, 2595 (2016).
[26] J. Tian, T.-F. Chung, I. Miotkowski, and Y. P. Chen, (2016), arXiv:1607.02651.
[27] In both experiments the currents are AC and the values provided in the text are the r.m.s. values. In the setup used in Ref.[18] a big fraction of the current flows through the bulk of the TI and the ferromagnetic metal (Py) placed on top of the TI, whereas in the setup used in Ref.[19], in optimal conditions, most of the current flows through the TI's surfaces.
[28] S. J. Haigh, A. Gholinia, R. Jalil, S. Romani, L. Britnell, D. C. Elias, K. S. Novoselov, L. A. Ponomarenko, A. K. Geim, and R. Gorbachev, Nature Materials **11**, 764 (2012).
[29] K.-H. Jin and S.-H. Jhi, Phys. Rev. B **87**, 075442 (2013).
[30] J. R. Wallbank, M. Mucha-Kruczyński, and V. I. Fal'ko, Phys. Rev. B **88**, 155415 (2013).
[31] J. Zhang, C. Triola, and E. Rossi, Phys. Rev. Lett. **112**, 096802 (2014).
[32] H. Steinberg, L. A. Orona, V. Fatemi, J. D. Sanchez-Yamagishi, K. Watanabe, T. Taniguchi, and P. Jarillo-Herrero, Phys. Rev. B **92**, 241409 (2015).
[33] G. Bian, T.-F. Chung, C. Chen, C. Liu, T.-R. Chang, T. Wu, I. Belopolski, H. Zheng, S.-Y. Xu, D. S. Sanchez, N. Alidoust, J. Pierce, B. Quilliams, P. P. Barletta, S. Lorcy, J. Avila, G. Chang, H. Lin, H.-T. Jeng, M.-C. Asensio, Y. P. Chen, and M. Z. Hasan, 2D Materials **3**, 021009 (2016).
[34] L. A. Ponomarenko, R. V. Gorbachev, G. L. Yu, D. C. Elias, R. Jalil, A. A. Patel, A. Mishchenko, A. S. Mayorov, C. R. Woods, J. R. Wallbank, M. Mucha-Kruczynski, B. A. Piot, M. Potemski, I. V. Grigorieva, K. S. Novoselov, F. Guinea, V. I. Fal'Ko, and A. K. Geim, Nature **497**, 594 (2013).
[35] C. D. Spataru and F. Léonard, Phys. Rev. B **90**, 085115 (2014).
[36] P. Lee, K.-H. Jin, S. J. Sung, J. G. Kim, M.-T. Ryu, H.-M. Park, S.-H. Jhi, N. Kim, Y. Kim, S. U. Yu, K. S. Kim, D. Y. Noh, and J. Chung, ACS Nano **9**, 10861 (2015).
[37] S. Rajput, Y.-Y. Li, M. Weinert, and L. Li, ACS Nano **10**, 8450 (2016).
[38] Z. Ren, A. A. Taskin, S. Sasaki, K. Segawa, and Y. Ando, Phys. Rev. B **82**, 241306 (2010).
[39] J. Xiong, A. C. Petersen, D. X. Qu, Y. S. Hor, R. J. Cava, and N. P. Ong, Physica E **44**, 917 (2012).
[40] T. Arakane, T. Sato, S. Souma, K. Kosaka, K. Nakayama, M. Komatsu, T. Takahashi, Z. Ren, K. Segawa, and Y. Ando, Nature Comm. **3**, 636 (2012).
[41] B. Xia, P. Ren, A. Sulaev, P. Liu, S. Q. Shen, and L. Wang, Phys. Rev. B **87**, 085442 (2013).
[42] K. Segawa, Z. Ren, S. Sasaki, T. Tsuda, S. Kuwabata, and Y. Ando, Phys. Rev. B **86**, 075306 (2012).
[43] Y. Xu, I. Miotkowski, C. Liu, J. Tian, H. Nam, N. Alidoust, J. Hu, C.-K. Shih, M. Z. Hasan, and Y. P. Chen, Nature Physics **10**, 956 (2014).
[44] C. Durand, X.-G. Zhang, S. M. Hus, C. Ma, M. A. McGuire, Y. Xu, H. Cao, I. Miotkowski, Y. P. Chen, and A.-P. Li, Nano Letters **16**, 2213 (2016).
[45] Y. Xu, I. Miotkowski, and Y. P. Chen, Nat Commun **7** (2016).
[46] C. Lee, F. Katmis, P. Jarillo-Herrero, J. S. Moodera, and N. Gedik, Nature Communications **7**, 12014 (2016).
[47] F. Katmis, V. Lauter, F. S. Nogueira, B. A. Assaf, M. E. Jamer, P. Wei, B. Satpati, J. W. Freeland, I. Eremin, D. Heiman, P. Jarillo-Herrero, and J. S. Moodera, Nature **533**, 513 (2016).
[48] W. Yang, S. Yang, Q. Zhang, Y. Xu, S. Shen, J. Liao,

J. Teng, C. Nan, L. Gu, Y. Sun, K. Wu, and Y. Li, Applied Physics Letters **105**, 092411 (2014).

[49] N. A. Sinitsyn, A. H. MacDonald, T. Jungwirth, V. K. Dugaev, and J. Sinova, Phys. Rev. B **75**, 045315 (2007).

[50] D. Kim, S. Cho, N. P. Butch, P. Syers, K. Kirshenbaum, S. Adam, J. Paglione, and M. S. Fuhrer, Nature Physics **8**, 459 (2012).

[51] H. Beidenkopf, P. Roushan, J. Seo, L. Gorman, I. Drozdov, Y. S. Hor, R. J. Cava, and A. Yazdani, Nature Physics **7**, 939 (2011).

[52] Q. Li, E. Rossi, and S. Das Sarma, Phys. Rev. B **86**, 235443 (2012).

[53] D. Culcer, E. H. Hwang, T. D. Stanescu, and S. Das Sarma, Phys. Rev. B **82**, 155457 (2010).

[54] N. P. Butch, K. Kirshenbaum, P. Syers, A. B. Sushkov, G. S. Jenkins, H. D. Drew, and J. Paglione, Phys. Rev. B **81**, 241301 (2010).

[55] Strictly speaking the value $\kappa_0 = 1$ is only valid for the case of a magnetically doped TI. However, given the large static dielectric constant of the TI, the error made by approximating the FM's dielectric constant by the vacuum's is negligible. For EuS, the suggested insulating FM, $\kappa_0 \approx 10$ giving an effective average dielectric constant $\kappa = 55$, instead of the used $\kappa = 50$.

[56] E. H. Hwang, S. Adam, and S. Das Sarma, Phys. Rev. Lett. **98**, 186806 (2007).

[57] C. Triola and E. Rossi, Phys. Rev. B **86**, 161408 (2012).

[58] S. Das Sarma and F. Stern, Phys. Rev. B **32**, 8442 (1985).

[59] K. Nomura and A. H. MacDonald, Phys. Rev. Lett. **98**, 076602 (2007).

[60] E. Rossi and S. Das Sarma, Phys. Rev. Lett. **101**, 166803 (2008).

[61] E. Rossi, S. Adam, and S. D. Sarma, Phys. Rev. B **79**, 245423 (2009).

[62] C.-P. Lu, M. Rodriguez-Vega, G. Li, A. Luican-Mayer, K. Watanabe, T. Taniguchi, E. Rossi, and E. Y. Andrei, PNAS **113**, 6623 (2016).

[63] J. Lopes dos Santos, N. Peres, and A. Castro Neto, Phys. Rev. Lett. **99**, 256802 (2007).

[64] R. Bistritzer and A. H. MacDonald, Proc. National Acad. Sciences United States Am. **108**, 12233 (2011).

[65] E. J. Mele, Journal of Physics D Applied Physics **45**, 154004 (2012).